Applied Catalysis B: Environmental 150–151 (2014) 411–420

Contents lists available at ScienceDirect

Applied Catalysis B: Environmental

journal homepage: www.elsevier.com/locate/apcatb

Probing significant light absorption enhancement of titania inverse opal films for highly exalted photocatalytic degradation of dye pollutants

Min Wu[a,b], Jing Liu[a], Jun Jin[a], Chao Wang[a], Shaozhuan Huang[a], Zhao Deng[a], Yu Li[a,**], Bao-Lian Su[a,b,c,*]

[a] Laboratory of Living Materials at the State Key Laboratory of Advanced Technology for Materials Synthesis and Processing, Wuhan University of Technology, 122 Luoshi Road, 430070 Wuhan, Hubei, China
[b] Laboratory of Inorganic Materials Chemistry (CMI), University of Namur, 61 rue de Bruxelles, B-5500 Namur, Belgium
[c] Department of Chemistry and Clare Hall College, University of Cambridge, Lensfield Road, Cambridge, UK

ARTICLE INFO

Article history:
Received 20 October 2013
Received in revised form
16 December 2013
Accepted 19 December 2013
Available online 27 December 2013

Keywords:
TiO_2
Inverse opal
Photonic crystal
Slow photon
Photocatalytic activity

ABSTRACT

The continuous titania inverse opal (TiO_2-IO) films have been prepared by sol–gel infiltration method and calcined at different temperatures. The morphologies of the TiO_2 inverse opal films remain unchanged under high temperature treatment. XRD patterns reveal an anatase crystalline phase between 550 and 900 °C and a mixture of anatase and rutile phase at 1000 °C. Comparing with the mesoporous TiO_2 films obtained under the same conditions, all the TiO_2 inverse opal films demonstrate a highly enhanced photocatalytic activity in photodegradation of rhodamine B (RhB) as dye pollutant model in aqueous solution. In spite of the fact that the TiO_2 inverse opal films with open macroporous structures and possible light scattering effect of the wavelengths can result in the higher photocatalytic activity in the degradation of the dye pollutant, the phenomenon of the slow photon occurring in the TiO_2 inverse opal photonic crystals can explain the extraordinary enhancement of the photocatalytic activity. In consequence, the TiO_2-IO-700, TiO_2-IO-550 and TiO_2-IO-800 films show the best photocatalytic performance mainly due to the slow photon effect at the light incident angle at 0°, 20° and 45°, respectively, a direct proof of light absorption enhancement due to the slow photon effect. The slow photon effect in TiO_2 inverse opals to enhance light absorption and further to enhance photocatalysis is very important for further potential applications in solar cells and other processes linked to the light absorption.

1. Introduction

During the last decades, TiO_2 has been expected to be the most promising photocatalyst in environmental applications, such as the photodegradation of organic pollutants and the purification of water and air [1–3]. To achieve high photodegradation efficiency of the pollutants, various methods have been carried out to improve the activity of TiO_2 by controlling the morphologies [4], doping anions and cations [5], modification of surface with metals and graphene [6–8] and exposing high surface energy facets [9,10]. TiO_2 aerosol [11–13], meso/nanoporous TiO_2 [14–16] and photonic materials [17–20] have also been used for efficient photodegradation of organic pollutants due to the good mass transport and high surface area.

For the photocatalytic process, it is well known that when a photon with energy of $h\nu$ matches or exceeds the band gap energy (E_g) of the semiconductor, an electron is excited from the valence band to the conduction band, leaving a hole behind. These charge carriers migrate to the surface and react with the chemicals adsorbed on the surface to decompose these chemicals. Generally, the photocatalytic activity of a semiconductor is mainly determined by three factors: the light absorption properties; the light excited charges (electron–hole pairs) transport rate and the electron–hole recombination rates on the surface [1–3]. As mentioned above, a lot of works have been reported on accelerating the electron–hole separation and transport to enhance the photocatalytic activity [21–24]. Most of the previous works on light absorption focused on broadening the absorption of TiO_2 to visible light [25–28]. Another possible way to reinforce the light absorption property, however less explored, is the increase of the path length of light to improve the photocatalytic efficiency, a structure effect other than

* Corresponding author. Tel.: +86 27 87855322/+32 81 724531; fax: +86 27 87879468/+32 81 725414.
** Corresponding author. Tel.: +86 27 87855322; fax: +86 27 87879468.
E-mail addresses: yu.li@whut.edu.cn (Y. Li), bao-lian.su@unamur.be, bao-lian.su@fundp.ac.be (B.-L. Su).

0926-3373/$ – see front matter © 2013 Elsevier B.V. All rights reserved.
http://dx.doi.org/10.1016/j.apcatb.2013.12.037

chemical composition effect. Several studies show that the hierarchically macro-mesoporous TiO_2 structures exhibit an important light harvesting effect of the macrochannels allowing light waves to penetrate deeper inside the photocatalyst [29–32]. For example, the efficiency of dye-sensitized solar cells can be improved by increasing the path length of light on these macro-mesoporous structures [33]. Recently, the macroporous TiO_2 inverse opals (TiO_2-IO) have been intensively studied in photocatalysis since this kind of structure can provide easy mass transportation and high surface area because of the hierarchical porous structure resulting in enhanced photocatalytic activity [31,32,38]. However one of the most important properties of macroporous inverse opal materials is less explored. In fact, these structures are photonic crystal structures having a periodic dielectric contrast and can provide an immense potential to increase the path length of light [34–38]. The feature of the photonic crystals (PCs) can allow to modulate the light propagation in the structures. In the length scale of the wavelength of light, light with certain energies is forbidden to propagate in the PCs because of coherent Bragg diffraction. This leads to stop-band reflection (also called photonic band gap, PBG) and the reflected energies (wavelength) depend on the periodic and dielectric contrast of the photonic crystals. At the frequency edges of the stop bands, photons propagate with strongly reduced group velocity in solid matter leading to the slow photon appearance. The slow photons can be observed at the edges (red and blue edges) of any stop band. The frequencies of slow photons can be thus varied depending on the edges frequencies (both at red and blue edges) of the stop bands of the photonic crystal. The location of stop bands, in consequence, the location of the red and blue edges depends on the photonic crystal structures when the chemical composition of two phases forming the photonic crystal structures is defined. This light reflectance and slow photons are generated by a structure effect. With the same chemical composition, by changing the air sphere diameter, the stop band position can be modulated. However, whether these slow photons can be used to enhance the light absorption or not depending on a specific condition: the wavelength of slow photons (at red or blue edge) overlaps with the electronic excitation wavelength (electronic band gap frequency) of semiconducting materials and the applied irradiation light wavelength. When these three wavelengths fall at the same wavelength zone, i.e. the condition cited above is satisfied, an enhancement of the light absorption by these slow photons can be expected and these slow photons will excite electrons of semiconducting materials from valence band to conduction band with the generation of a large number of electron–hole pairs resulting in an enhanced photocatalytic activity [34–38]. If the above condition is not satisfied, i.e. only two of three wavelengths coincide no slow photon enhanced light absorption effect can be observed. For example, if the red or blue edge wavelength of stop band coincides with the irradiation wavelength zone, however the electron excitation wavelength (electron excitation band gap) is located at a different wavelength, no photon at red and blue edges can be used to excite the electron. The occurrence of slow photon effect depend thus also on the irradiation wavelength and electronic band gap of materials. The irradiation wavelength can be easily adjusted following the position of red and blue edges and electronic band gap of materials. The stop band can be tuned by the variation of materials and also by changing the incident angle.

Although the materials containing an inverse opal structure have been previously and largely used in the photocatalysis by different research groups [32], the photocatalysis enhancement is often attributed to porous structure of materials. The slow photon concept in photonic crystals (inverse opals) to enhance light absorption and further to enhance photocatalysis is rarely explored although some papers claimed slow photon effect. Only few papers demonstrated the slow photon effect in photocatalysis enhancement [34]. The application of slow photon concept is a great challenge.

At present, the most typical method in preparation of TiO_2-IO films is based on a three step method: deposition of opals on a substrate by the self-assembly of submicrospheres (silica or polymeric) from a colloidal suspension; then filtration of titanium precursor into the interstitial spaces of the opal; finally removal of the colloidal crystal template by solvent extraction or calcination [39–41]. Although many achievements have been obtained for the TiO_2-IO films preparation, there are seldom reports on the effect of thermal treatment temperatures on the photocatalytic activity of the TiO_2-IO films. Furthermore, it will be interesting to investigate how the slow photon effect happens and influences the photocatalytic activity. In addition, the slow photon effect has been proved only in gas phase photocatalysis, the reaction performed in aqueous solution can render the modulation of slow photon effect more difficult due to the fact that the slow photon effect can become weaker in aqueous environment because of the lower refraction index contrast between TiO_2 wall and the aqueous-filled voids. However, for environmental remediation using photocatalytic technology, the processes occur very often in aqueous solution. Thus how to benefit the slow photon effect of photonic crystals is of great challenge in aqueous environment. Herein, we report the photocatalytic activity of titania inverse opal films calcined at different temperatures in the photodegradation of rhodamine B (RhB) in aqueous solution and correlated with the photonic properties of TiO_2-IO films. An evident slow photon effect on enhancement of the photocatalytic activity has been noted with the light incident angle change.

2. Experimental

2.1. Fabrication of TiO_2-IO films

The TiO_2-IO films were prepared based on the previous work with a slight modification [41]. Briefly, 8 mL of styrene (previously washed 3 times with 2 M NaOH aqueous solution to remove the inhibitor) and 120 mL of water were heated to 70 °C under N_2 atmosphere. $K_2S_2O_8$ (0.07 g) was added to initiate the reaction which was stopped after 3 h by cooling down the container. The polystyrene (PS) spheres opals were obtained on a 4 cm^2 quartz slide (20 mm × 20 mm × 1 mm) by the vertical deposition. The solution was prepared by mixing 100 μL of titanium (IV) isopropoxide (TTIP) in mixture of 10.0 mL anhydrous ethanol and 2 μL hydrochloric acid and then was stirred for 5 min for a fully dispersion of titanium isopropoxide. One droplet of the solution was carefully deposited on the middle of the PS opal. The template was then exposed to air and dried at room temperature for 12 h. The infiltration process was repeated three times in order to increase the filling of the voids. The resulting TiO_2/PS composites were then calcined in air at 300 °C with a ramp rate of 2 °C/min. This temperature was maintained for 2 h and then subsequently raised to 550, 700, 800, 900 or 1000 °C at 2 °C/min, respectively. After 3 h, the thermal treatment process was stop and the oven was cooled down to room temperature. The quartz substrates covered by the TiO_2 inverse opal were characterized. The mesoporous TiO_2 films were prepared by dropping the titanium isopropoxide, ethanol and hydrochloric acid solution on the quartz slide with the same procedure described above.

2.2. Photocatalytic activity measurement

The photocatalytic activities of the TiO_2-IO films and mesoporous TiO_2 films were evaluated by the degradation of a model pollutant basic RhB. The samples were placed at the bottom of a beaker filled with 1×10^{-5} M RhB aqueous solution

(10 mL, PH = 9.5) in the dark for 1 h to allow the RhB adsorbing onto the film surface. The photodegradation of RhB was initiated and conducted by UV–vis light irradiation (250 nm–800 nm, PLS-SXE-300UV, Beijing). At every 10 min interval, a solution of 1 mL was taken out. The absorption spectrum of the solution was then recorded with a UV2550 (SHIMADZU) UV–vis spectrometer. After every analysis, the analyzed liquid was quickly poured back into the beaker to ensure a roughly equivalent volume of solution. The efficiency of RhB degradation was calculated with the following equation of $E_f = (C_0 - C)/C_0 \times 100\%$, Where C_0 is the calculated initial RhB solution and C is the final measured value of the degraded RhB solution. The cycling performance was also carried out to examine the photocatalytic stability of the TiO_2-IO films: the films were rinsed with water after each test and dried at 80 °C for next utilization.

2.3. Characterization

X-ray diffraction (XRD) patterns were obtained with a Bruker Advanced 8 using Cu Kα radiation (λ = 1.54056 Å). Field emission scanning electronic microscopy (FESEM) was performed on a Hitachi S-4800 with an accelerating voltage of 15 kV. Transmission electronic microscopy (TEM) and high resolution transmission electronic microscopy (HRTEM) were performed on a JEOL JEM-2100F operating at 200 kV. The reflection spectra were obtained on an Avaspec 2048/2 fiber-optic spectrometer by measuring the reflectance spectra of the film at normal incidence in water. The TGA and DSC curves were recorded by using a thermal analyzer (Setaram Labsys Evo) in air atmosphere with temperature ramp of 5 °C/min. The absorption spectra were collected with a UV2550 (SHIMADZU) UV–vis spectrometer. For measurements, the TiO_2 powders were scratched from the inverse opal films and crashed to fine powder to destroy the inverse opal structure and to avoid the effect of inverse opal structure on the absorption spectra and then dispersed in distilled water by ultrasonication for several minutes with a concentration of 0.025 mg/mL.

3. Results and discussion

3.1. XRD, SEM, TEM and HRTEM characterizations of the TiO_2-IO films

PS spheres with radius of 250 nm were selected in this experiment. Exploring only the calcination temperature effects by the single diameter of PS spheres can exclude other factor effects in this experiment, such as the quantity of materials. Fig. 1a clearly shows the PS spheres were self-assembled in a face centered cubic (fcc) structure with the (1 1 1) close-packed surface on the top. The insert in Fig. 1a is an ordinary photograph of the self-assembled PS opal template through the vertical method. To select the calcination temperature for removal of the PS spheres and detect the carbon residue or doping in final TiO_2, TGA and DSC were recorded with the PS/TiO_2 precursor. Fig. S1 shows the corresponding TGA and DSC curves of PS/TiO_2 composite. Three weight losses have been noticed in the temperature range of room temperature to 220 °C, 220–400 °C and 400–510 °C. The first weight loss around 3 wt% corresponds to the removal of ethanol and water from composite. The second and third weight losses, both of which are exothermic, can be attributed to successive oxidative degradation of PS spheres. All the PS spheres can be removed at around 510 °C. Over this temperature, no further weight loss can be detected. Particularly, the DSC curve also shows no exothermal peaks between 510 and 900 °C,

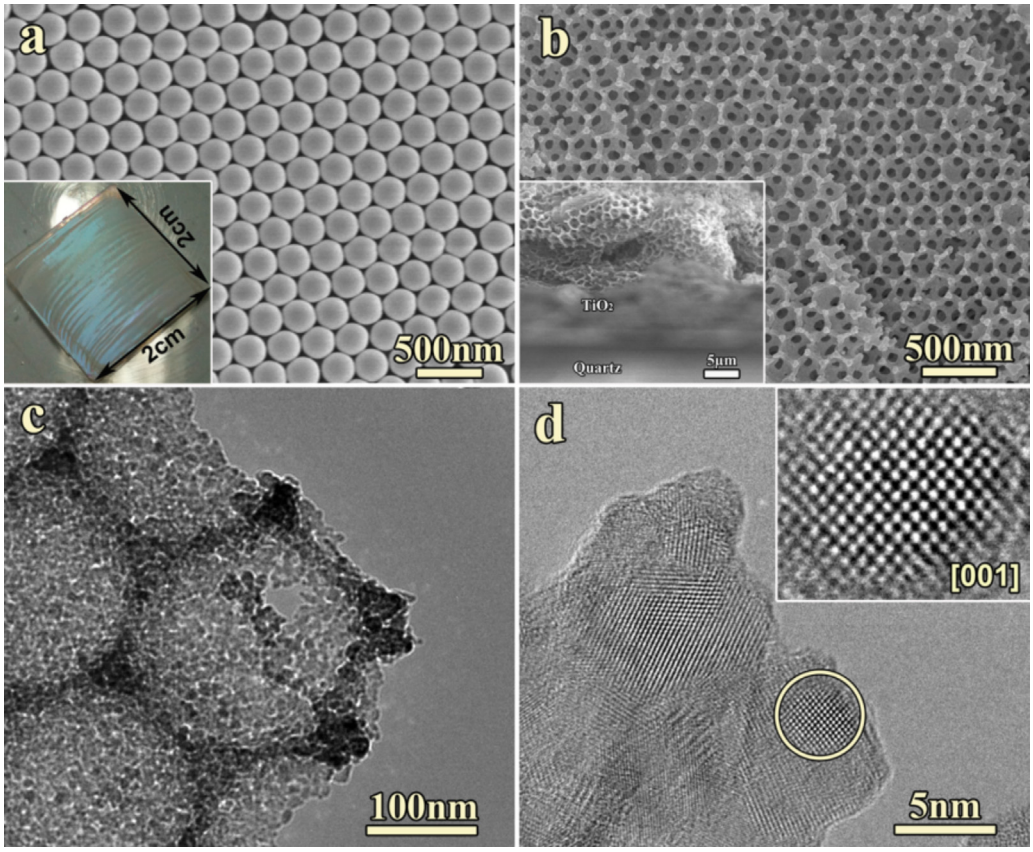

Fig. 1. Electron microscopy images of the PS template and TiO_2-IO-550. (a) SEM image of PS opal template; (b) SEM image of TiO_2-IO-550; (c) low magnification TEM image of TiO_2-IO-550; (d) HRTEM image of the TiO_2-IO-550. The insert in (a) is the ordinary photo of the film, in (b) is the cross section of the film and in (d) is the enlarged area of the circled particle viewed along c axis of anatase of titania.

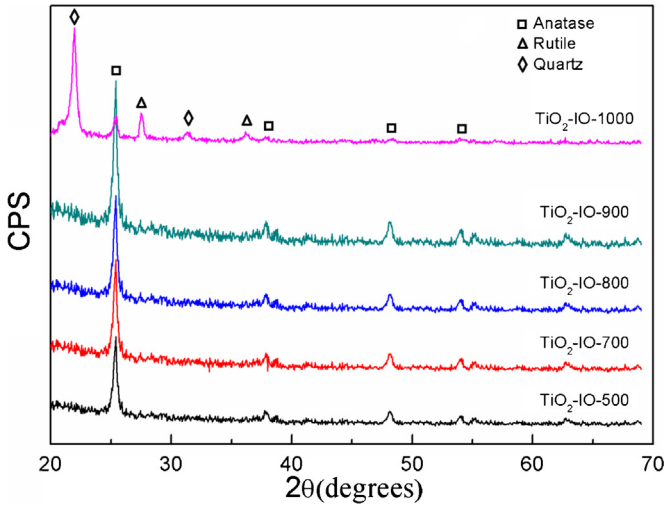

Fig. 2. The XRD results of the TiO_2-IO film obtained at different calcination temperatures.

indicating no carbon residue or doping in TiO_2. Thus the first calcination temperature was selected at 550 °C. Above 900 °C, there is an exothermal trend from 920 °C, which should be the beginning of phase conversion from anatase to rutile. Fig. 1b demonstrates the SEM image of the sample calcined at 550 °C (then designated as TiO_2-IO-550, the same for other samples). It obviously shows the face centered cubic (fcc) structure. The diameter of air spheres is ca. 195 nm, indicating a shrinkage of about 22% when compared to the original colloidal crystal template. This shrinkage results in a substantial isotropic compressive stress on the crystal that can cause the break-up of the photonic film and lead to the appearance of defects. The insert in Fig. 1b is the cross section of the inverse opal film, which shows the thickness of the film is around 5 μm. Fig. 1c shows the TEM image of the TiO_2-IO-550 sample. The diameter of air spheres is 192 nm according to the TEM observations, which is similar to the SEM observations on the air pore diameter. The nanocrystallites of inverse opal are randomly assembled into worm-like mesopores, which can provide more active sites for photodegradation. Most of the crystallites are around 10 nm in size. HRTEM image (Fig. 1d) clearly shows that there are still some amorphous TiO_2 around the nanoctrystallites indicating a low crystallization of the nanoparticles. The insert in Fig. 1d displays the HRTEM image of one nanoparticle, which corresponds to the anatase phase of TiO_2 along *c* axis.

The X-ray diffraction (XRD) patterns of the TiO_2-IO film calcined at different temperatures are shown in Fig. 2. The results show that only anatase of TiO_2 can be obtained at 700, 800 and 900 °C. The sample obtained at 1000 °C is the mixture of anatase and rutile of TiO_2, which is in consistence with the DSC curve, where an exothermal trend can be observed at 920 °C (Fig. S1), indicating the conversion of anatase phase to rutile phase. The broadening of the peaks in the XRD pattern indicates that the product has nanoscale dimensions. These results obtained using titanium isopropoxide as precursor are different from the previous data obtained using titanium ethoxide as precursor [41]. In the previous work using titanium ethoxide, the rutile phase appeared after calcination at 700 °C while our present work showed the appearance of rutile at 1000 °C. The hydrolysis speed of titanium isopropoxide is lower than that of titanium ethoxide in this system due to the addition of hydrochloric acid. Faster hydrolysis can lead to faster crystallization under thermal treatment resulting in earlier phase transformation.

Fig. 3 displays the SEM images of the inverse opal samples calcined at 700, 800, 900 and 1000 °C, respectively. These images show that the high quality of inverse opals is maintained after high temperature treatment, indicating that the 3D macroporous materials are stable under high temperatures. However, intensive SEM observations reveal that part of the inverse opal structure has been distorted after the calcination at high temperatures, in particular at 1000 °C. The thermal stability of the 3D macroporous material is very important for photocatalytic performance regarding to the utilization of slow photon effect in photonic crystals. Nevertheless, the disordered structure may bring higher chemical activity because of more active sites induced by disordered structure. The diameters of air spheres show a down-shift from 195 nm to 155 nm with increasing calcination temperatures due to the contraction (Table 1). TEM observations of the samples demonstrate that the diameters of the nanocrystallites increase from 19 nm at 700 °C to 80 nm at 1000 °C (Table 1). No amorphous TiO_2 has been found in all these samples indicating a good crystallization of the nanoparticles. The increase in nanocrystallite size due to the nanoparticle crystallization and inverse opal framework contraction should be the main reason for the decrease of air spheres diameter.

3.2. The absorption spectra of TiO_2-IO films

It is well known that the optical absorption property is relevant to the electronic structure feature in determining a semiconductor's photocatalytic activity [42]. UV–vis spectrophotometry is then used to reveal the energy structures and the optical absorption properties of the obtained TiO_2-IO samples. Fig. 4a shows the absorption spectra of the TiO_2-IO films obtained at different calcination temperatures. The absorption spectra of inverse opal samples prepared below calcination temperatures of 800 °C are similar. The band gap energy can be estimated from the intersect point between the tangent line of the steep curve and the wavelength axis after the original absorption data has been subjected to Urbach's rule. Then the equation $(\alpha E_{photon})^2 = K(E_{photon} - E_g)$ is applied to evaluate the band gap of the TiO_2-IO films, where α is the absorption coefficient, E_{photon} is the discrete photon energy, K is a constant, and E_g is the band gap energy [43,44]. The plot of $(\alpha E_{photon})^2$ vs. E_{photon} is shown in Fig. 4b. The extrapolated value (the dash lines to the x axis) of E_{photon} at $\alpha = 0$ gives absorption edge energy corresponding to E_g, which are listed in Table 1. The samples at calcination temperatures below 800 °C show the similar band gap energy of 3.13 eV (corresponding to the wavelength of 396 nm), whilst the sample calcined at 1000 °C shows the band gap energy of 3.06 eV (corresponding to the wavelength of 405 nm) due to the mixture of anatase and rutile phases and larger crystallite size. All electronic band gaps of the samples demonstrate slight shift to a higher wavelength comparing to the bulk TiO_2 [2], which is similar to our previous work [38a]. However, according to the quantum confinement effects, the nanocrystallites of TiO_2 should make the band gap energy shift to lower wavelength. It may be related to crystal structure alterations during the calcination process [38a]. Further experimental work should be carried out to reveal this phenomenon.

3.3. The reflectance spectra of TiO_2-IO films

The reflectance spectra are very important to understand the position of photonic band gap (PBG) of the photonic crystal structures. Fig. 5a is the reflectance spectra of the prepared TiO_2-IO films at an incident light angle of $\theta = 0°$. The reflectance peaks in the spectra correspond to the PBG wavelengths of the structure. The PBG wavelength is related to the air sphere size of the TiO_2-IO films. Table 1 demonstrates the PBG wavelengths of the samples. The PBG positions are blue shift with increasing calcination temperatures. The position of the reflection peak (λ_p) can be calculated using Bragg's law [41] and depends directly on the air sphere size of the photonic crystals when other factors remain unchanged. It

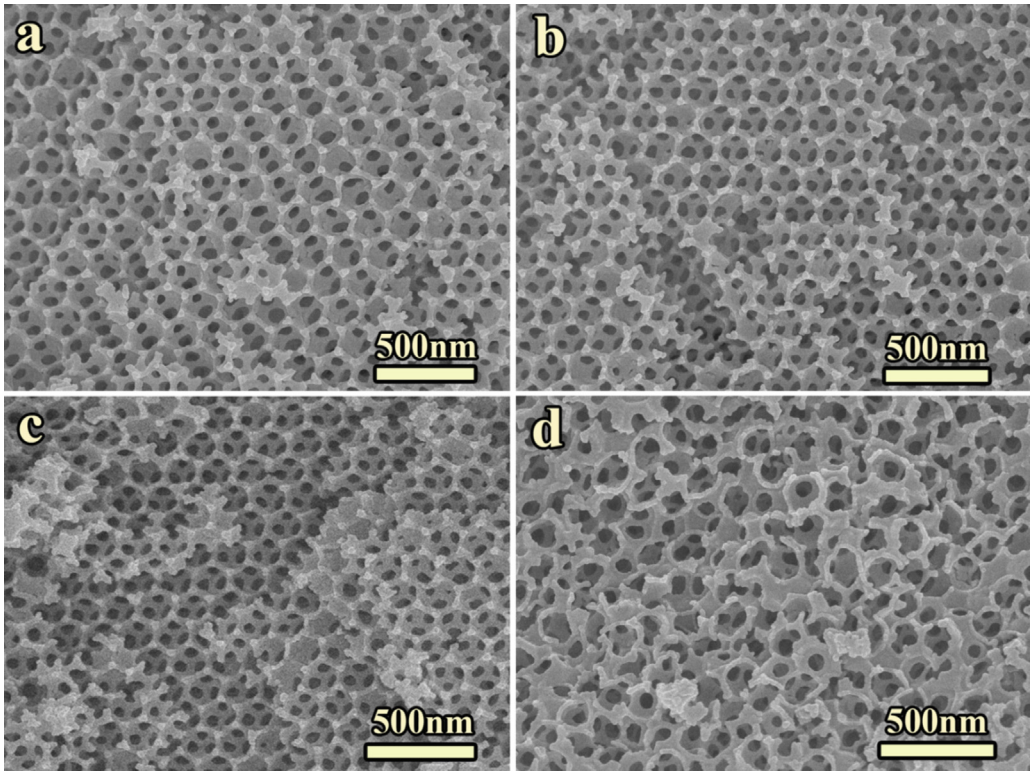

Fig. 3. The SEM images of the inverse opal films at different calcined temperatures. (a) the TiO_2-IO-700; (b) the TiO_2-IO-800; (c) the TiO_2-IO-900; (d) the TiO_2-IO-1000.

is interesting to note that a shoulder with the maximum at around 385 nm, which is very close to the electronic absorbance of the sample (396 nm, Table 1 and Fig. 4b), is observed at the blue edge of the stop band of the sample TiO_2-IO-700. This indicates that the reflection of the incident light is partly suppressed by the strong light absorption at around 385 nm by TiO_2 material. This strong absorption vanishing part of light reflection at around electronic band gap of TiO_2 could be very important for photocatalysis, since if the incident light is reflected due to the photonic stop band at material absorption wavelength, no electrons can be promoted from valence band to conduction band, being unfavorable for photocatalysis.

For a high quality photonic structure, its PBG can be tuned by changing the angle between the incident light and the films and following Bragg's law [41]. Increasing the light incident angle can result in a blue shift response of the reflectance peak to low wavelength. In other words, the blue shift of PBG wavelength observed as a function of incident light angle change can confirm the real photonic structure of the films [41,45,46]. The angle between the incident light and the films has been tuned to 20° and 45° in this experiment. Fig. 5b and c shows the reflectance spectra at $\theta = 20°$ and $\theta = 45°$, respectively, which obviously demonstrate the blue shift of all the PBG wavelength comparing to the spectra at $\theta = 0°$ (Fig. 5a). Table 1 lists all the observed experimental peaks and Fig. 5d depicts the variation of PBG position (wavelength) as a function of calcination temperatures. It is clear that all the samples decrease their PBG wavelength with increasing light incident angle, showing good quality of all the TiO_2-IO films. The blue shift with increasing calcination temperatures is well in line with decreasing the air sphere size. It is worthy to mention that although the photonic structure becomes more disordered after calcination at 900 and 1000 °C, the PBGs are observed, indicating that TiO_2-IO-900 and TiO_2-IO-1000 still present the photonic structure feature. For TiO_2-IO-550 film, when the angle between the incident light and the film increases to 20°, a shoulder with the maximum at around 385 nm is also observed showing a strong light absorption around the electronic band gap of TiO_2. The shoulder disappears after increasing the incident angle to 45°. The photonic stop band of TiO_2-IO-700 film is blue-shifted toward 408 nm when the incident angle

Table 1
The structure parameters of the TiO_2 inverse opal films and mesoporous TiO_2 films.

Samples	Crystalline grains size (nm)	Band gap (eV)	Pore diameter (nm)	$\Delta\lambda/\lambda_p \times 100\%$	λ_p (nm)[a]		
					0°	20°	45°
TiO_2-IO-550	~10	3.13	~195	14.2	448	430	390
TiO_2-IO-700	~19	3.13	~185	16.5	426	408	366
TiO_2-IO-800	~20	3.13	~165	16.8	392	376	341
TiO_2-IO-900	~50	3.11	~160	21.2	375	364	332
TiO_2-IO-1000	~80	3.06	~155	22.4	369	358	325
m-TiO_2-550	~6	3.15	–	–	–	–	–
m-TiO_2-700	~15	3.13	–	–	–	–	–
m-TiO_2-800	~18	3.14	–	–	–	–	–
m-TiO_2-900	~35	3.11	–	–	–	–	–
m-TiO_2-1000	~67	3.08	–	–	–	–	–

[a] The peaks of the reflectance spectra of the film were collected in water. "–" Means no data obtained.

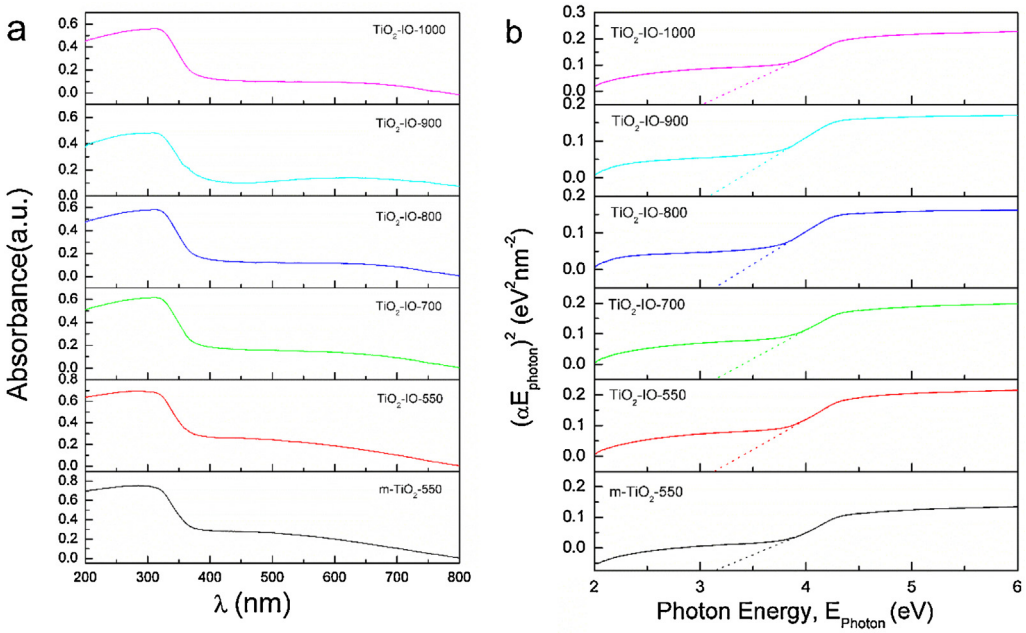

Fig. 4. (a) UV/Vis absorption spectra of the different samples. (b) Plots of $(\alpha E_{photon})^2$ vs. E_{photon} curve for the calculation of the band gap energy for the different samples.

increases to 20°. Note that a shoulder can still be observed at around 385 nm, but is largely reduced comparing to that of $\theta = 0°$. The still observed shoulder at around 385 nm should be related to the intrinsic structure of inverse opal, such as crystallinity, crystalline structure, crystallite size and defects. The reduced shoulder means that slow photon may happen here in spite of light reflection due to the fact that photonic stop band dominates over the light absorption. With increasing the incident angle to 45°, no shoulder can be seen, meaning that the light reflection due to PBG effect dominates the light absorption of bulk material. Concerning the films of TiO_2-IO-800, TiO_2-IO-900 and TiO_2-IO-1000, no shoulder phenomenon is observed. However, the reflection spectra of TiO_2-IO-900 and TiO_2-IO-1000 demonstrate long tailing peaks comparing to other films. Most possibly, it is due to the appearance of more disordered structure in the films because of high temperature treatment.

As stated in above paragraph, it is also possible to evaluate the quality of the inverse opal by comparing the fractional bandwidth ($\Delta\lambda/\lambda_p$) of these samples from the reflectance spectra: a peak broadening effect can be attributed to disorder within the structure [41,45–48]. $\Delta\lambda$ is the full width at half maximum and λ_p is the position of the maximum reflectance of the peak. For a given dielectric contrast of material, the fractional bandwidth depends only on the crystal structure. Thus it is an ideal parameter for comparing the uniformity of different samples. The lower $\Delta\lambda/\lambda_p$ value corresponds to the better quality of opal films. Table 1 lists the $\Delta\lambda/\lambda_p$ values of the samples obtained at different temperatures. The samples of TiO_2-IO-550, TiO_2-IO-700 and TiO_2-IO-800 show a relatively low value indicate good quality of the photonic crystals. The higher values of TiO_2-IO-900 and TiO_2-IO-1000 should be directly related to the appearance of short-range cracks, which is in agreement with the SEM observations. Furthermore, the disordered structure was really amplified with the angle tuning demonstrating long tailing peaks for the two samples (Fig. 5b and c).

3.4. The photocatalytic activity of TiO_2-IO films

The photodegradation of RhB in aqueous solution was explored by using these TiO_2-IO films calcined at different temperatures. To differentiate between the photocatalysis and just the photolysis of RhB, experiments were also carried out in the absence of photocatalyst. Fig. 6a shows the results of the photodegradation of RhB on TiO_2-IO films at incident light angle of $\theta = 0°$. It obviously shows that without photocatalyst, only an insignificant degradation (less than 2%) of RhB was observed after 60 min irradiation.

The sample TiO_2-IO-700 demonstrates the best photodegradation RhB at $\theta = 0°$ with an extraordinarily high RhB degradation rate. After 60 min of UV–vis light irradiation, about 97% of RhB was degraded on TiO_2-IO-700, which is significantly much more efficient than other inverse opal films. Generally, the smaller crystallites size of catalysts can result in a better catalytic activity because of high surface area and more active sites. Furthermore, the smaller grain can reduce the rate of recombination of electrons and holes resulting in the photocatalytic efficiency enhancement [48,1]. As the band gap energies of TiO_2-IO-900 and TiO_2-IO-1000 are lower than that of TiO_2-IO-700, these two samples should have wider light wavelength utilization at the same reaction conditions. However, the photocatalytic activity of these two samples is still lower than that of TiO_2-IO-700. It seems that the larger crystalline grain sizes dominate the activity in this case. The much lower activity of TiO_2-IO-550 can be ascribed to the low crystallization of the nanoparticles leading to low transport of the electrons and holes to surface. However, it is hard to explain the low activity of TiO_2-IO-800 film. After all, both TiO_2-IO-700 and TiO_2-IO-800 films have very similar inverse opal structure, crystal phase, crystalline grain size and band gap energy (Table 1). Most probably, the low photocatalytic activity of TiO_2-IO-800 and high photocatalytic activity of TiO_2-IO-700 should be caused by the slow photon effect according to the reflectance spectra obtained at different incident light angles (Fig. 5).

Generally, light primarily localizes in the high dielectric part of the photonic crystals at the red edge and in the low dielectric medium at the blue edge. Light at red edge will interact more strongly with the high dielectric medium (TiO_2 in this case) and less strongly at the blue edge resulting in the fact that slow photon effect often occurs at red edge of the PBG. If the red edge of the PBG of titania inverse opal films could be coupled to the electronic band gap of TiO_2, this theoretically should enhance UV light absorption by the semiconductor, which in turn should enhance the photocatalytic activity of TiO_2 by increasing charges formation.

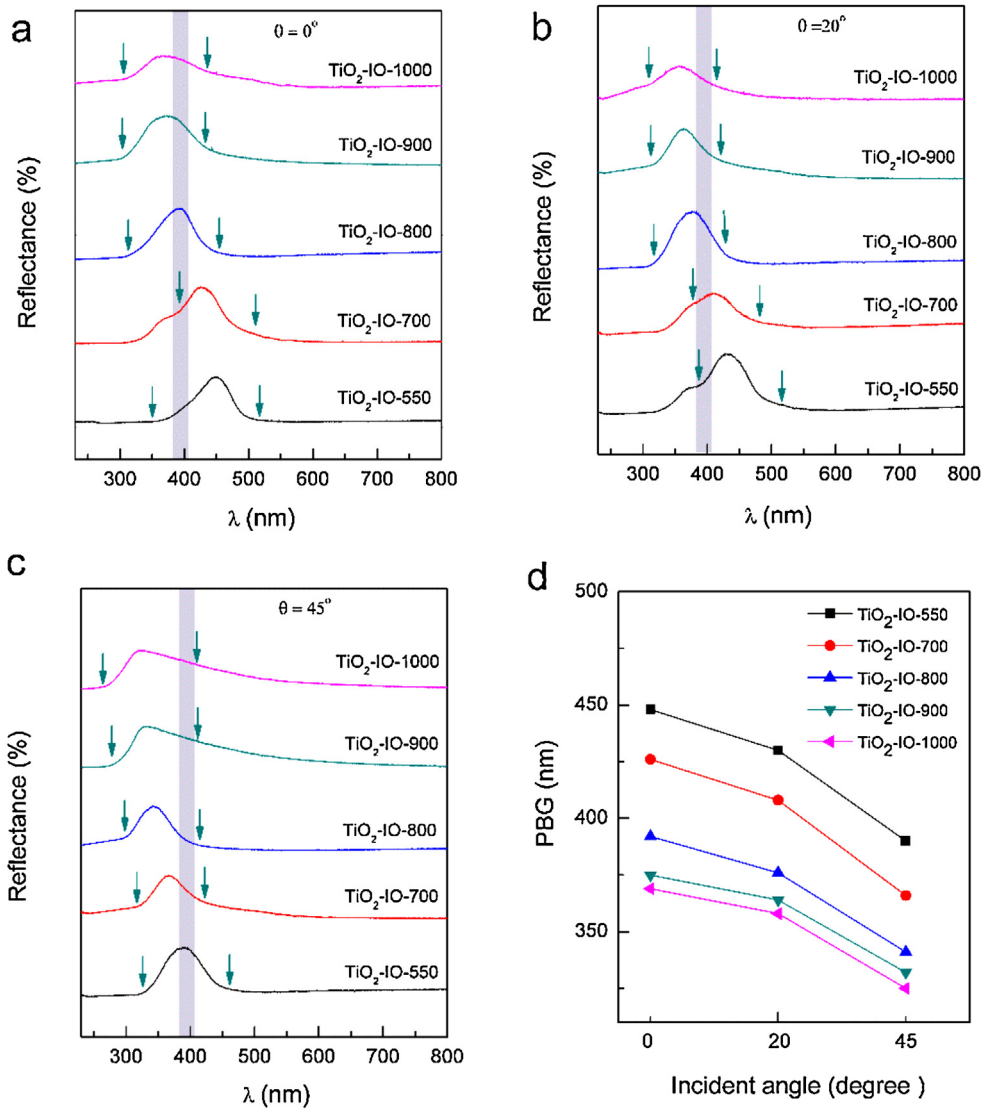

Fig. 5. Reflectance spectra of the TiO_2-IO films calcined at different temperatures in water with different light incident angles: (a) $\theta = 0°$; (b) $\theta = 20°$; (c) $\theta = 45°$. (d) the variation of PBG as function of calcination temperatures. The gray region in (a), (b) and (c) represents the electronic band gap of the TiO_2-IO films and the arrows are the positions of blue (left) and red (right) edges of the PBG. (For interpretation of the references to color in this figure legend, the reader is referred to the web version of the article.)

Nevertheless, it was observed that because of the non-perfectly regular inverse opal structure of the synthesized samples, the slow photon can also happen at the blue edge of the PBG to enhance the photocatalytic activity of TiO_2 although it was not clearly claimed [34].

In addition, there are two competing effects in the photocatalysis activity for photonic crystals: the slow photon enhancement and the high reflectivity of the stop band suppression. Previously theoretical calculation demonstrated that the suppression will reduce the photoactivity due to the fact that the stop band is much wider than the enhanced activity region brought by slow photon [50]. However, the characters resulting from the photonic band structure can highly be suppressed by the absorption of the materials [51]. If the reflectivity is suppressed due to high absorption, while at the same time the blue or red edge used for enhancement still resides in a sufficiently transparent region, the slow photon induced light absorption enhancement will improve the photocatalytic activity [34].

Table 1 and Fig. 4b show that the samples of TiO_2-IO-550, TiO_2-IO-700 and TiO_2-IO-800 demonstrate the electronic excitation wavelength at around 396 nm. The samples of TiO_2-IO-900 and TiO_2-IO-1000 show the electronic excitation wavelength at around 399 and 405 nm, respectively. At the light incident angle $\theta = 0°$, only TiO_2-IO-700 film demonstrates a strong absorption at around 385 nm (Fig. 5a), which couples very well with the electronic band gap of TiO_2, resulting in the higher photocatalytic activity than other samples. For the samples of TiO_2-IO-550, TiO_2-IO-900 and TiO_2-IO-1000, no obvious absorption appears in the reflectance spectra. The photocatalytic activity depends mainly on hierarchically macro-mesoporous structure, the particle sizes, the phases, crystallinity of particles and the active sites or defect sizes. The synergism of these factors results in different photocatalytic activity of three samples. For the sample of TiO_2-IO-800, the electronic excitation wavelength is around 396 nm and the PBG is around 392 nm. It is reasonable that the reflectivity of the light will reduce light absorption in the photocatalytic process demonstrating a suppression of the activity because of the wide stop band (Table 1 and Fig. 5a).

The photonic band gap of the inverse opal can be tuned by changing the angle between the incident light and the films [34,41]. Increasing the angle resulting in the reflectance peak blue shift to low wavelength can highly modify the photocatalytic activity

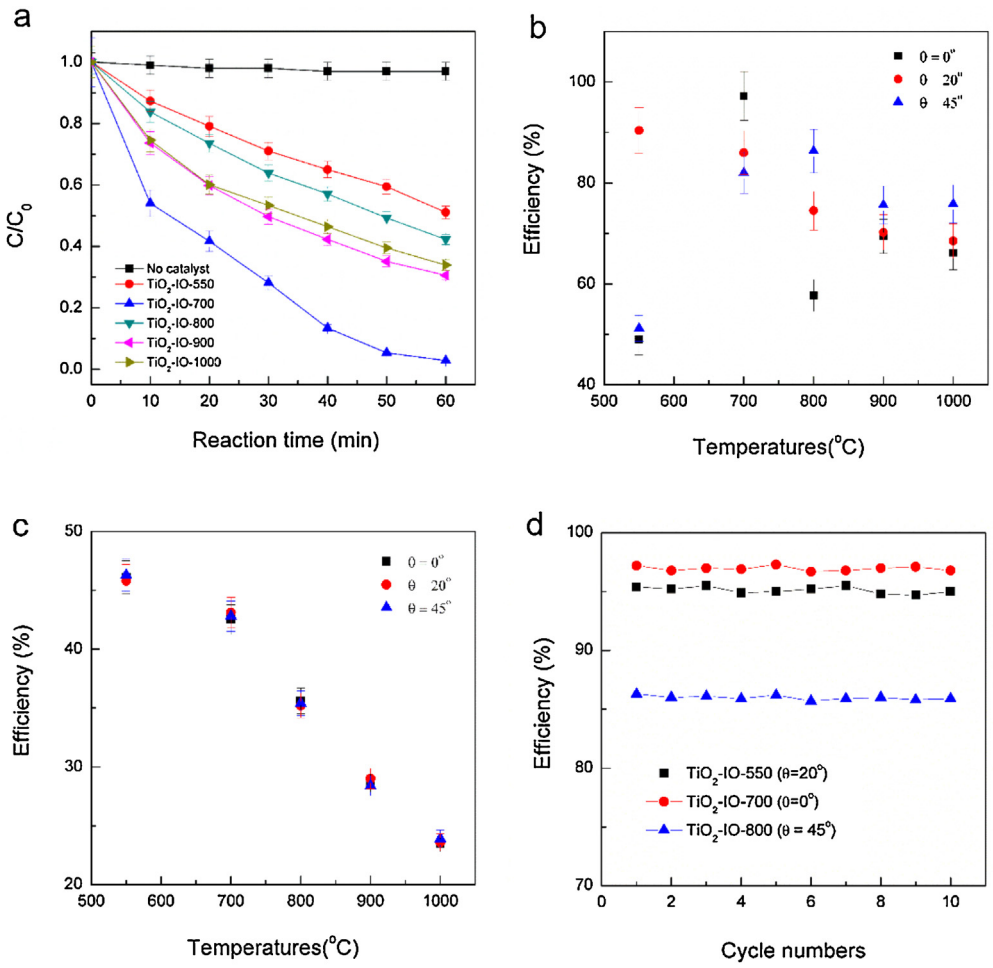

Fig. 6. (a) Photodegradation of RhB solution on the different TiO_2-IO films obtained at different calcination temperatures. (b) The efficiencies of the photodegradation of RhB on TiO_2-IO films and (c) mesoporous TiO_2 films ($\theta = 0^\circ$, $\theta = 20^\circ$ and $\theta = 45^\circ$) calcined at different temperatures. (d) Cycling performance of the photocatalytic efficiency on the TiO_2-IO-550 ($\theta = 20^\circ$), TiO_2-IO-700 ($\theta = 0^\circ$) and TiO_2-IO-800 at ($\theta = 45^\circ$).

of the samples. If the photocatalytic activity is truly modified by changing the light incident angle, the slow photon effect is thus clearly proved since whatever the light incident angle is, all these parameters which can affect the photocatalytic activity such as the mass transport properties due to the porous structure, defect sites, particle size effect, charge diffusion facility owing to necking effect between crystallites and crystallinity of TiO_2-IO remain unchanged. The incident light angle has been tuned to 20° and then 45° to compare the catalytic of the inverse opal films. Fig. 6b shows the comparison of the photocatalytic activities of the samples at $\theta = 0^\circ$, $\theta = 20^\circ$ and $\theta = 45^\circ$. As shown in Fig. 5b, the reflectance curves of TiO_2-IO-550 at $\theta = 20^\circ$ displays a strong absorbance at around 385 nm, indicating a slow photon effect induced an enhancement of the photocatalytic activity. The photocatalytic activity of TiO_2-IO-550 demonstrating a greatly catalytic activity increase verifies the slow photon induced light absorption enhancement. Although the PBG position is blue shifted, a slight deduced absorption of sample TiO_2-IO-700 at around 385 nm (Fig. 5b) close to the PBG still indicates slow photon occurring. However, the slow photon cannot greatly enhance the photocatalytic activity because the PBG can counteract part of the slow photon effect. Thus the photocatalytic activity of TiO_2-IO-700 at $\theta = 20^\circ$ is lower than those of TiO_2-IO-550 at $\theta = 20^\circ$ and TiO_2-IO-700 at $\theta = 0^\circ$ (Fig. 6b). The samples of TiO_2-IO-800, TiO_2-IO-900 and TiO_2-IO-1000 show an enhancement of the photocatalytic activity due to the blue shift of reflectance peaks resulting in slow photon effect appearance at the red edge of PBG. And the sample of TiO_2-IO-800 shows a higher enhancement of photocatalytic activity mainly due to the retained better photonic structure (Fig. 6b).

At the incident light angle of $\theta = 45^\circ$, the photocatalytic activity of TiO_2-IO-550 displays a big decrease due to the reflectivity (Figs. 5c and 6b). However, the sample of TiO_2-IO-800 demonstrates the highest photocatalytic activity at $\theta = 45^\circ$ because of the slow photon effect happening at the red edge of the PBG. And both the photocatalytic activity of TiO_2-IO-900 and TiO_2-IO-1000 demonstrate a slight enhancement. It is interesting to note that although the sample of TiO_2-IO-700 shows a very slight decrease of the performance due to the blue shift of the reflectance peak, the photocatalytic activity is still higher than that of other three samples of TiO_2-IO-550, TiO_2-IO-900 and TiO_2-IO-1000 due to the slow photon effect happening at the red edge of the PBG.

The angle changing clearly verifies that the slow photon effect occurs and can greatly affect the photocatalytic activity of the inverse opal films. Although there is obvious amorphous TiO_2 observed on the particles, the sample TiO_2-IO-550 shows the highest performance at $\theta = 20^\circ$ because of the strong absorption at the blue edge of PBG but demonstrates great decrease at $\theta = 45^\circ$ because of the reflectivity domination. The sample TiO_2-IO-700 demonstrates the highest performance at $\theta = 0^\circ$ and high performance at $\theta = 20^\circ$ due to the strong absorption at the blue edge of the PBG. Still, the sample TiO_2-IO-700 has high performance at $\theta = 45^\circ$ because of the slow photon effect at the red edge of the PBG. The sample TiO_2-IO-800 shows the lowest performance at $\theta = 0^\circ$ due to the reflectivity domination, whilst it shows the enhanced

photocatalytic activity with the incident light angle increase and shows the highest performance at $\theta = 45^\circ$ due to the slow photon effect at the red edge of the PBG. For the samples of TiO_2-IO-900 and TiO_2-IO-1000, it is possible that the more disordered structures in the inverse opal structure counteracting part of the slow photon effect should be a main reason of the low photocatalytic activity increase.

The photocatalytic activity of the mesoporous TiO_2 film (m-TiO_2) synthesized under the same conditions was also evaluated to confirm the photonic structures effect. Without the slow photon effect in the mesoporous film, the photocatalytic activity should be lower than that of the inverse opal with the same TiO_2 loadings. In particular, the photocatalytic activity will not change with the incident light angle increasing. Fig. S2 demonstrates the typical TEM images of the mesoporous TiO_2 film calcined at 550 °C, indicating a mesoporous structure with inter-particular porosity and revealing a rather narrow particle size of 6 nm in diameter. TEM observations of other m-TiO_2 samples show that the diameters are similar to the crystalline sizes of the TiO_2-IO films at the corresponding temperature (Table 1). Furthermore, the band gap energies of the m-TiO_2 samples (Table 1) also demonstrate similar band gap energies comparing to the inverse opal structure. Fig. 6c also compares the photocatalytic activity of the mesoporous TiO_2 films at light incident angle $\theta = 0^\circ$, 20° and 45°, respectively. As expected, the mesoporous film sample calcined at 550 °C demonstrates the best photocatalytic activity. The photocatalytic activity of all the mesoporous samples calcined at different temperatures is lower than the inverse opals. Specifically, the photocatalytic activity does not change with the incident light angles increasing for the mesoporous TiO_2 film although the electronic excitation band gap is quite similar to TiO_2-IO films and good connection between crystallites with good necking effect which facilitates the charge diffusion across crystallites. All the above findings confirm that the slow photon effect happens and enhances the photocatalytic activity of the TiO_2 inverse opal photonic crystals. Except for the slow photon effect, hierarchically macro-mesoporous structures, defect sites, particle size and crystallinity of TiO_2 also contribute to the photocatalytic activity. The synergism of these factors results in TiO_2-IO-700 having the best photocatalytic activity at $\theta = 0^\circ$. And the samples of TiO_2-IO-550 and TiO_2-IO-800 show the best photocatalytic activity at incident light angle of 20° and 45°, respectively.

Moreover, the cycling performance of the TiO_2-IO-550 at $\theta = 20^\circ$, TiO_2-IO-700 at $\theta = 0^\circ$ and TiO_2-IO-800 at $\theta = 45^\circ$ were carried out in this experiment (Fig. 6d). The results demonstrate that all the three samples demonstrate good cycling performance. After 10 recycles, there is no obvious photocatalytic activity loss, indicating the high stability of the inverse opal structure. The high stability of the inverse opal is very important for waste water treatment and for further potential applications, such as in solar cells and photonic water splitting.

4. Conclusion

The continuous TiO_2-IO films treated at different temperatures have been obtained. XRD patterns reveal that only anatase of TiO_2 can be obtained with calcination temperatures between 550 and 900 °C and a mixture of anatase and rutile of TiO_2 appears with calcination temperature at 1000 °C. The photocatalytic activity of the TiO_2-IO films treated at different temperatures by photodegradation of RhB aqueous solution has been investigated. Due to the slow photon effect of the TiO_2 inverse opal photonic crystals, the samples of TiO_2-IO-700, TiO_2-IO-550 and TiO_2-IO-800 demonstrates the best photocatalytic activity at incident light angle of 0°, 20° and 45°, respectively. However, the disordered structures and large crystalline grain sizes of TiO_2-IO-900 and TiO_2-IO-1000 only result in a slight enhancement of photocatalytic activity. This work demonstrated that by modulating the ordered macroporous inverse opal structures and incident light angle the light absorption can be enhanced and further photocatalytic activity can be highly exalted. The present work can be a good example and of importance for the enhancement of light absorption for all the processes relating to light absorption such as solar cells and optical communications.

Acknowledgements

This work is realized in the frame of a program for Changjiang Scholars and Innovative Research Team (IRT1169) of Chinese Ministry of Education and an Interuniversity Attraction Poles Program (Inanomat-P6/17)-Belgian State-Belgian Science Policy and the frame of Interreg IV (France-Wallonie). B. L. Su acknowledges the Chinese Central Government for an "Expert of the State" position in the Program of the "Thousand Talents" and Ministry of Education for a "Changjiang" scholarship at the Wuhan University of Technology and the Clare Hall College and the Department of Chemistry, University of Cambridge, for a Clare Hall Life Member and the financial support, respectively. Y. Li acknowledges Hubei Provincial Department of Education for the "Chutian Scholar" program. This work is also financially supported by the Ph.D. Programs Foundation of Ministry of Education of China (20120143120019), Wuhan Youth Chenguang Program of Science and Technology (2013070104010003), the Fundamental Research Funds for the Central Universities (2012-II-004) and Self-determined and Innovative Research Funds of the SKLWUT (2013-ZD-6).

Appendix A. Supplementary data

Supplementary data associated with this article can be found, in the online version, at http://dx.doi.org/10.1016/j.apcatb.2013.12.037.

References

[1] A. Hagfeldt, M. Gratzel, Chem. Rev. 95 (1995) 49.
[2] X. Chen, S.S. Mao, Chem. Rev. 107 (2007) 2891.
[3] Y. Li, X.Y. Yang, Y. Feng, Z.Y. Yuan, B.L. Su, Crit. Rev. Solid State Mat. Sci. 37 (2012) 1.
[4] (a) Z.Y. Yuan, B.L. Su, Chem. Commun. (2002) 1202;
(b) Z.Y. Yuan, J.F. Colomer, B.L. Su, Chem. Phys. Lett. 363 (2002) 362;
(c) Z.Y. Yuan, B.L. Su, Colloids Surf. A 241 (2004) 173.
[5] M.R. Hoffmann, S.T. Martin, W. Choi, D.W. Bahnemann, Chem. Rev. 95 (1995) 69.
[6] H. Zhang, X.J. Lv, Y. Wang, J.H. Li, ACS Nano 4 (2010) 380.
[7] V. Subramanian, E.E. Wolf, P.V. Kamat, J. Am. Chem. Soc. 126 (2004) 4943.
[8] Y. Xie, K.L. Ding, Z.M. Liu, R.T. Tao, Z.Y. Sun, H.Y. Sun, H.Y. Zhang, G.M. An, J. Am. Chem. Soc. 131 (2009) 6648.
[9] H.G. Yang, C.H. Sun, S.Z. Qiao, J. Zou, G. Liu, S.C. Smith, H.M. Cheng, G.Q. Lu, Nature 453 (2008) 638.
[10] G. Liu, H.G. Yang, X. Wang, L. Cheng, J. Pan, G.Q. Lu, H.M. Cheng, J. Am. Chem. Soc. 131 (2009) 12868.
[11] M.R. Ayers, A.J. Hunt, Mater. Lett. 34 (1998) 290.
[12] M. Schneider, A. Baiker, Catal. Today 35 (1997) 339.
[13] Z. Zhu, M. Lin, G. Dagan, M. Tomkiewicz, J. Phys. Chem. 99 (1995) 15950.
[14] J.C. Yu, L. Zhang, J. Yu, New J. Chem. 26 (2002) 416.
[15] M.H. Bartl, S.P. Puls, J. Tang, H.C. Lichtenegger, G.D. Stucky, Angew. Chem. Int. Ed. 43 (2004) 3037.
[16] Q. Dai, L.Y. Shi, Y.G. Luo, J.L. Blin, B.L. Su, J. Photochem. Photobiol. A 148 (2002) 295.
[17] B.T. Holland, C. Blanford, A. Stein, Science 281 (1998) 538.
[18] W. Dong, H. Bongard, B. Tesche, F. Marlow, Adv. Mater. 14 (2002) 1457.
[19] Z.Z. Gu, A. Fujishima, O. Sato, Angew. Chem. Int. Ed. 41 (2002) 2067.
[20] X.D. Wang, E. Graugnard, J.S. King, Z.L. Wang, C.J. Summers, Nano Lett. 4 (2004) 2223.
[21] W. Choi, A. Termin, M.R. Hoffmann, J. Phys. Chem. 98 (1994) 13669.
[22] K. Maeda, Y. Shimodaira, B. Lee, K. Teramura, D.L. Lu, H. Kobayashi, K. Domen, J. Phys. Chem. C 111 (2007) 18264.
[23] Y.X. Zhao, X.F. Qiu, C. Burda, Chem. Mater. 20 (2008) 2629.
[24] J. Xu, B.F. Yang, M. Wu, Z.P. Fu, Y. Lv, Y.X. Zhao, J. Phys. Chem. C 114 (2010) 15251.

[25] C. Burda, Y.B. Lou, X.B. Chen, A.C.S. Samia, J. Stout, J.L. Gole, Nano Lett. 3 (2003) 1049.
[26] X.B. Chen, Y.B. Lou, A.C.S. Samia, C. Burda, J.L. Gole, Adv. Funct. Mater. 15 (2005) 41.
[27] R. Asahi, T. Morikawa, T. Ohwaki, K. Aoki, Y. Taga, Science 293 (2001) 269.
[28] M. Sathish, B. Viswanathan, R.P. Viswanath, C.S. Gopinath, Chem. Mater. 17 (2005) 6349.
[29] X.Y. Li, L.H. Chen, Y. Li, J.C. Rooke, C. Wang, Y. Lu, A. Krief, X.Y. Yang, B.L. Su, J. Colloid Interface Sci. 368 (2012) 128.
[30] Y. Li, Z.Y. Fu, B.L. Su, Adv. Funct. Mater. 22 (2012) 4634.
[31] Y. Lu, H.T. Yu, S. Chen, X. Quan, H.M. Zhao, Environ. Sci. Tech. 46 (2012) 1724.
[32] (a) S. Meng, D.Z. Li, X. Zhang, J. Wang, J. Chen, J.L. Fang, S. Yu, X.Z. Fu, J. Mater. Chem. A 1 (2013) 2744;
(b) X.F. Chen, X.C. Wang, X.Z. Fu, Energy Environ. Sci 2 (2009) 872;
(c) X.C. Wang, J.C. Yu, C.M. Ho, Y.D. Hou, X.Z. Fu, Langmuir 21 (2005) 2552;
(d) S.L. Chen, A.J. Wang, C.T. Hu, C. Dai, J.B. Benziger, AIChE J. 58 (2011) 568.
[33] N. Hoffmann, Chem. Rev. 108 (2008) 1052.
[34] (a) J.I.L. Chen, G. von Freymann, S.Y. Choi, V. Kitaev, G.A. Ozin, Adv. Mater. 18 (2006) 1915;
(b) J.I.L. Chen, G.A. Ozin, J. Mater. Chem. 19 (2009) 2675;
(c) J.I.L. Chen, G. von Freymann, V. Kitaev, G.A. Ozin, J. Am. Chem. Soc. 129 (2007) 1196.
[35] F. Sordello, C. Duca, V. Maurinoa, C. Mineroa, Chem. Commun. 47 (2011) 6147.
[36] Y.Z. Li, T. Kunitake, S. Fujikawa, J. Phys. Chem. B 110 (2006) 13000.
[37] J. Liu, M. Li, J. Wang, Y. Song, L. Jiang, T. Murakami, A. Fujishima, Environ. Sci. Technol. 43 (2009) 9425.
[38] (a) M. Wu, Y. Li, Z. Deng, B.L. Su, ChemSusChem 4 (2011) 1481;
(b) M. Wu, A.M. Zheng, F. Deng, B.L. Su, Appl. Catal. B: Environ. 138–139 (2013) 219.
[39] J.D. Joannopoulos, Nature 414 (2001) 257.
[40] H. Cong, W. Cao, Langmuir 19 (2003) 8177.
[41] Y. Li, F. Piret, T. Léonard, B.L. Su, J. Colloid Interface Sci. 348 (2010) 43.
[42] J. Tang, Z. Zou, J. Ye, Chem. Mater. 16 (2004) 1644.
[43] S. Tsunekawa, T. Fukuda, A. Kasuya, J. Appl. Phys. 87 (2000) 1318.
[44] Y. Li, X.Y. Yang, J. Rooke, G. Van Tendeloo, B.L. Su, J. Colloid Interface Sci. 348 (2010) 303.
[45] R. Rengarajan, D. Mittleman, Phys. Rev. E 71 (2005) 016615.
[46] F. Piret, B.L. Su, Chem. Phys. Lett. 457 (2008) 376.
[47] Z. Zhou, X.S. Zhao, Langmuir 21 (2005) 4717.
[48] R.C. Schroden, M. Al-Daous, C.F. Blanford, A. Stein, Chem. Mater. 14 (2002) 3305.
[50] A. Mihi, H. Míguez, J. Phys. Chem. B 109 (2005) 15968.
[51] G. von Freymann, S. John, M. Schulz-Dolbrick, E. Vekris, N. Tetreault, S. Wong, V. Kitaev, G.A. Ozin, Appl. Phys. Lett. 84 (2004) 224.